Research Article Vol. 33, No. 22 / 3 Nov 2025 / Optics Express 45915
Optics EXPRESS

Leveraging Fresnel reflection of legacy PON to enhance distributed fiber vibration/temperature sensing

LIU MAOQI,[1,2] WANG JINGCHUAN,[2] LI YIBIN,[2] LIU CHEN,[1,3] ZHAO LUMING,[1] ALAN PAK TAO LAU,[2] YU CHANGYUAN,[2,4] AND LU CHAO[2]

[1]National Engineering Laboratory for Next Generation Internet Access System, School of Optical and Electronic Information, Huazhong University of Science and Technology, Wuhan 430074, China
[2]Photonics Research Institute, Department of Electrical and Electronic Engineering, The Hong Kong Polytechnic University, Hong Kong SAR, China
[3]liuchen@hust.edu.cn
[4]changyuan.yu@polyu.edu.hk

Abstract: Legacy fiber passive optical networks (PONs) require not only high-speed data access but also regular in-service monitoring. Optical time domain reflectometry (OTDR) is a fundamental technique for PON in-service monitoring. Traditional OTDR is limited to detecting fiber breakpoints along the feeder fiber, failing to achieve PON monitoring of the point-to-multipoint (P2MP) structure. In this work, we exploit the Fresnel reflection points in access networks as fiber-optic sensors for PON branch sensing. Linear frequency modulation (LFM)-based phase sensitive OTDR (φ-OTDR) is employed for distributed sensing and power profile estimation of the PON feeder fiber, while Fresnel reflections from fiber connectors are utilized for event detection and trace recognition in optical network unit (ONU) branches. The system achieves a spatial resolution of 1 m for distributed sensing along the feeder fiber, with a sensing sensitivity of 56 $p\varepsilon/\sqrt{Hz}$. The longitudinal power profile is also acquired by the averaging of the long-term φ-OTDR trace and indicates a fiber attenuation coefficient of 0.207 dB/km for the standard single-mode feeder fiber at 1550.13 nm. By adjusting the fiber lengths and the positions of the reference reflectors, traces from four distinct branches are recognized, and a spatial resolution of 0.2 m is achieved. Experimental results demonstrate the precise detection of fiber break points and bending loss, as well as the ability to monitor variations in strain and temperature. The system exhibits a vibration detection sensitivity of 93 $p\varepsilon/\sqrt{Hz}$, with a coefficient of 15.11 rad/mK for phase changes induced by temperature variations. In addition, we discuss the implementation of in-service PON monitoring based on the proposed scheme, comparing cost, feeder fiber sensing, and branch recognition performance with the existing OTDR-based PON monitoring schemes.

1. Introduction

Fiber-to-the-home (FTTH) technology has gradually become the mainstream choice for broadband access network [1]. Passive optical networks (PONs) are the primary implementation of FTTH [2]. In-service PON monitoring for anomalies and failures is important to ensure the continuous and reliable operation of customer communication services [3]. Optical time domain reflectometer (OTDR) is utilized to achieve physical layer monitoring in PON [4]. Conventional OTDR measures backscattered light by emitting pulsed light with high peak power and the spatial resolution of OTDR-based PON monitoring is determined by the pulse width. The scattered behaviors mainly include Rayleigh scattering and Fresnel reflection. However, OTDR can only detect simple events like fiber bending and break and fails to reconstruct the profile of

#572895 https://doi.org/10.1364/OE.572895
Journal © 2025 Received 10 Jul 2025; revised 8 Oct 2025; accepted 10 Oct 2025; published 21 Oct 2025

Optics EXPRESS

external disturbances effectively. Coherent correlation OTDR (CC-OTDR) has been proposed to achieve high-resolution PON monitoring and simultaneous monitoring of strain changes [5] and temperature changes [6]. This technique adopts coherent optical subassembly (COSA) to transmit pseudo-random binary sequences (PRBS), and the receiver employs signal autocorrelation to extract sensing information [7]. Nevertheless, this method is only suitable for detecting the segments near high-intensity Rayleigh scattering areas and Fresnel reflection points, lacking the ability to achieve distributed sensing along the entire PON feeder fiber. Employing each section of optical fiber as a sensor, phase-sensitive OTDR (φ-OTDR) can realize distributed optical fiber sensing (DFOS) [8,9], which is widely used in perimeter intrusion detection with high detection sensitivity and strong reliability [10]. φ-OTDR can also enhance spatial resolution by chirped pulses [11] and optical pulse coding [12], and even utilize real-time communication data streams to achieve distributed sensing [13,14]. However, the above techniques can only characterize a point-to-point (P2P) optical link, and the backscattering signals of different branches will overlap and affect event recognition in PON.

According to the multi-branch PON monitoring, a multi-wavelength scheme has been proposed, where each wavelength is assigned to monitor a specific branch [15]. However, it is highly costly and exhibits low spectral efficiency, making practical deployment challenging. An alternative solution is embedded OTDR, which integrates monitoring at the optical network unit (ONU) side, but becomes impractical in the event of a fiber break [16]. Additionally, machine learning techniques have been suggested for the recognition of OTDR traces and event localization across multiple branches [17]. To reduce the complexity of monitoring, the reference reflector is proposed to be used for monitoring multiple branches. The reference reflector should be identical in each fiber branch and is wavelength-selective [18,19]. Alternatively, non-wavelength-selective reference reflectors can be applied by adjusting the fiber length and the position of reflectors to avoid trace overlap. In this case, high-speed ultra-long pseudo-random noise (PN) sequences are proposed to achieve high-resolution multi-branch monitoring [20]. In addition, prior research has suggested a framework to concurrently enable optical fiber sensing and the monitoring of multiple branches via PON, introducing extra reflective semiconductor optical amplifiers (RSOAs) at each ONU branch [21].

In this paper, we employ a continuous linear frequency modulation (LFM) probe for PON in-service monitoring, enabling simultaneous distributed sensing of the PON feeder fiber and multi-branch event detection. Our approach harnesses previously unexploited Fresnel reflection points in existing access networks, utilizing the fiber span between two points as a fiber-optic sensor to enable robust branch sensing. Branch recognition requires prior knowledge of the branch connector distribution, which can be obtained directly from the ONU structure or initial calibrations. The coherent receiver utilizes a matched filter to achieve distributed vibration sensing of the feeder fiber and Fresnel-reflection-based event detection for individual ONU branches, including temperature variations, external vibrations, fiber breakpoints, and bending. Along the feeder fiber, polarization and interference fading are effectively mitigated through the division of multiple traces for the rotate-vector summed (RVS) algorithm [22], resulting in a spatial resolution of 1 m. Moreover, the longitudinal power profile (LPP) along the feeder fiber is obtained by performing long-term averaging. For ONU branches, a spatial resolution of 0.2 m is achieved by extracting Fresnel reflection signals from fiber connectors or manufacturing defects along ONU branches. The performance of distributed sensing and Fresnel reflection-based sensing is compared employing a continuous LFM probe, an LFM pulse probe, and a QPSK pulse probe, respectively. This approach allows the identification of fiber breakpoints and bending from multiple branches and enables the measurement of temperature and strain changes through phase variations at adjacent reflection points. Furthermore, the continuous sensing probe can be utilized as the carrier or occupy a dedicated wavelength channel to enable the monitoring of the PON feeder fiber and multiple branches during operation. Our method achieves distributed

Optics EXPRESS

sensing in PONs by utilizing Rayleigh backscattering (RBS) along the feeder fiber and discrete Fresnel reflection-based connector pairs as sensors in the branches, thereby ensuring the efficient operation and maintenance of access networks.

2. Theoretical analysis

For a conventional φ-OTDR system, the RBS field at a given position z along the fiber link can be expressed as a superposition of N scattering points within the sensing probe duration t_p:

$$E_{\mathrm{RBS}}(z,t) = \sum_{k=1}^{N} A_k e^{i(\omega t - 2\beta z_k)} \mathrm{rect}(\frac{t-\tau}{t_p}), \tag{1}$$

where A_k is the amplitude of the backscattering light from the k-th scattering point, τ is the temporal delay to the scattering point, ω is the angular frequency of the light, $\beta = 2\pi n/\lambda$ is the propagation constant (with n as the refractive index and λ as the wavelength), z_k is the position of the k-th scattering point. The factor $2\beta z_k$ accounts for the round-trip phase shift as the light travels to position z_k and back.

When a sequence signal $s(t)$ is employed as the sensing probe instead of a short pulse, the output at the receiving end can be represented in a convolution form. The received signal $r(t)$ is given by

$$r(t) = s(t) * h(t), \tag{2}$$

where the operator '$*$' represents the convolution operation, $h(t)$ is the impulse response of the fiber link, which is related to the RBS field in Eq. (1). To recover the impulse response $h(t)$, the received signal $r(t)$ must be processed with a matched filter. Specifically, the received signal can be correlated with the sequence signal $s(t)$, which can be expressed as

$$r_c(t) = r(t) \otimes s(t) = [s(t) \otimes s(t)] * h(t), \tag{3}$$

where $r_c(t)$ is the recovered signal after matched filter, and the operator '$\otimes$' represents the correlation operation.

In this configuration, the spatial resolution of φ-OTDR is determined by the full width at half maximum (FWHM) of the autocorrelation function of the sensing probe. For an LFM probe, the FWHM is inversely proportional to the frequency sweep bandwidth. Similarly, for a coded sequence such as quadrature phase-shift keying (QPSK), the FWHM of the main lobe of the autocorrelation function is determined by the signal bandwidth [14]. However, the sidelobes $n(t)$ of the autocorrelation function introduce noise, increasing crosstalk between different positions along the fiber.

Regarding the PON structure, the passive optical splitter (POS) serves as the interface connecting the optical line terminal (OLT) to individual ONUs, while the feeder fiber establishes the connection between the POS and the OLT, as shown in Fig. 1(a). To distinguish events across different ONU branches, fiber connectors in the branch between OLT and ONU are employed as reference reflectors, with the strong Fresnel reflection signals generated by these connector points and inherent fabrication defects acting as unique sensing markers. In φ-OTDR, events are typically detected by analyzing the phase difference of Rayleigh scattering signals from different fiber segments. In this approach, however, the phase difference between Fresnel reflections from two reflection points is utilized for event detection. Since the intensity of Fresnel reflection signals is significantly higher than that of Rayleigh scattering, this method enables simultaneous sensing while also serving as a marker for branch identification. As shown in Fig. 1(b), sensing probes are launched by a coherent transceiver and three fiber connectors (X, Y, Z) are located in the fiber link after circulator. X and Y are physical contact (UPC) connectors and Z is an open angled physical contact (APC) connector at the end to simulate the end-reflection from

Optics EXPRESS

the ONU. The connectors produce distinct peaks of the received trace after matched filtering at the receiver. The sensing probe can be launched as either a continuous signal or a pulsed signal from the transceiver, and it can be either an LFM signal or a random communication sequence. Perturbations in temperature and strain around the optical fiber induce changes in the refractive index. The phase shift of the transmitted signal between two discrete sensing points (X and Y) is correlated with the refractive index variation and can be mathematically expressed as

$$\Delta\varphi_{XY} = 2\int_{X}^{Y} d(\beta z) = \frac{4\pi n\xi}{\lambda}\Delta z + \frac{4\pi z}{\lambda}\Delta n \tag{4}$$

where $\Delta\varphi_{XY}$ denotes the phase shift. The first term of Eq. (4) represents the phase change induced by vibrations due to strain variations, where ξ is the elasto-optic coefficient, and Δz denotes the change in fiber length caused by the vibration. The second term accounts for the phase change induced by temperature variations, with Δn representing the change in refractive index resulting from the temperature variation. By extracting the phase traces corresponding to the positions of these peaks and calculating $\Delta\varphi_{XY}$, external perturbations in temperature and strain can be quantitatively obtained.

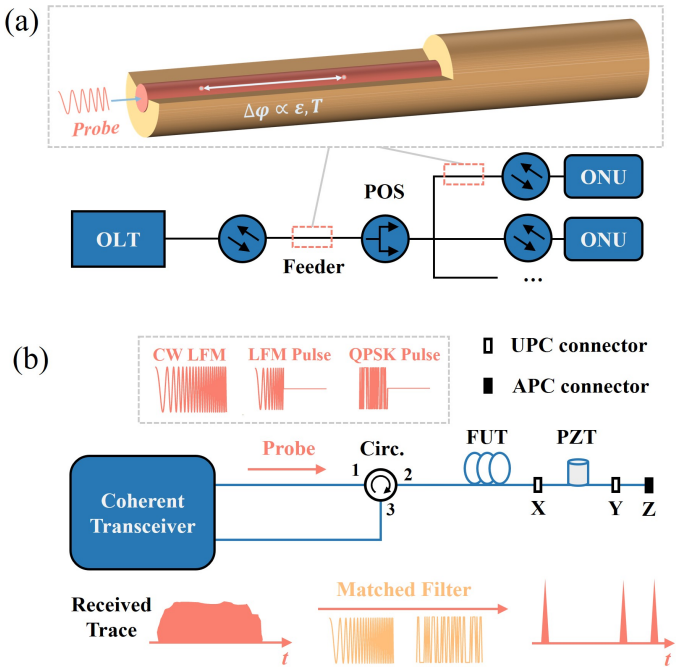

Fig. 1. (a) Combined fiber sensing mechanism in PON.(b) φ-OTDR system with matched filter and fiber connectors. PZT: piezoelectric transducer, FUT: fiber under test.

3. Experimental results and discussion

3.1. P2P experiment

We construct an experimental setup following the schematic diagram, as shown in Fig. 2. Light from a narrow-linewidth laser (NLL, NKT E15) operating at 1550.13 nm is split into two paths using a polarization-maintaining optical coupler. One path serves as the local oscillator (LO) and is directed into an integrated coherent receiver (ICR, NeoPhotonic Class 40), while the other path is fed into an IQ modulator. A continuous 500 MHz LFM signal generated by an

Optics EXPRESS

arbitrary waveform generator (AWG, Keysight 8190A) is employed as the sensing probe. The continuous probe is amplified by an EDFA and subsequently passed through an optical bandpass filter (OBPF) to suppress amplified spontaneous emission (ASE) noise. The filtered probe then enters the 9.8-km feeder fiber via a circulator. A 10-m piezoelectric transducer (PZT) is placed between reference reflectors X and Y to simulate a 500-Hz vibration. A continuous LFM signal with a starting frequency of 70 MHz and a bandwidth of 500 MHz is transmitted into a 9.8-km fiber under test (FUT). The received signal from the circulator passes through another EDFA and OBPF, then enters the ICR for dual-polarization coherent detection. Four low-pass filters (LPFs, 1 GHz bandwidth) are connected after the ICR to suppress high-frequency noise. Subsequently, the four channels are fed into a real-time oscilloscope (RTO, Keysight DSAZ594A) with a sampling rate of 1.25 GS/s for data acquisition. Figure 3(a) illustrates the intensity trace near the vibration position, where three distinct intensity peaks correspond to the three connectors. Then the corresponding phase traces are extracted in Fig. 3(b). Phase difference is calculated among these three points in Fig. 3(c) and the phase differences between X-Z and X-Y accurately reconstruct the vibration waveform, indicating strong signal fidelity in these channels. In contrast, the Y-Z phase difference shows minimal response, with only faint periodic variations observable. These variations are likely due to spatial leakage from the X-Y path, where vibrational signals inadvertently influence the Y-Z region. Besides, we can also detect the vibration based on Rayleigh scattering employing the digital signal processing (DSP) of φ-OTDR. Figure 3(d) compares the power spectral densities (PSDs) of the vibration traces extracted from Fresnel reflections ($\Delta\varphi_{XY}$ and $\Delta\varphi_{XZ}$) and the vibration trace obtained from φ-OTDR. It can be observed that the signal-to-noise ratios (SNRs) of these traces are consistent, with a noise floor of -51 dB rad^2/Hz, corresponding to a detection sensitivity of 32 p$\varepsilon/\sqrt{\text{Hz}}$ [23]. To investigate the sensing performance under different probes, we utilize the IQ modulator to transmit an LFM probe with a duty cycle of 3.03% and a sweep bandwidth of 500 MHz, and a QPSK probe with the same duty cycle and bandwidth, respectively. Figure 4(a) presents the autocorrelation functions (ACFs) of the QPSK probe and LFM probe. It can be observed from the zoom-in view that both probes maintain nearly identical full width at half maximum (FWHM) for their main lobes. The ACF of the QPSK probe exhibits a significantly higher sidelobe noise floor compared to the LFM probe, where the sidelobe power decreases rapidly beyond the main lobe. We control the input average power of all three probes to be 0 dBm before entering the circulator. Figure 4(b) illustrates the traces obtained after matched filtering. Despite the identical input power, the trace of the continuous LFM probe exhibits the highest SNR. This is because the extinction ratio of the IQ modulator is relatively low and pulsed probes introduce instability of the automatic bias controller in the IQ modulator. Additionally, the transient effects of the erbium-doped fiber amplifier (EDFA) and its amplification of noise in non-signal time slots further degrade the performance. The intensities of the RBS traces induced by the pulsed QPSK and LFM probes are similar. However, the noise floor of the QPSK trace is noticeably higher than that of the LFM trace, which aligns with the analysis based on the ACFs.

Traditional PONs typically connect multiple ONUs, ranging from 16 to 128 [24], to a single OLT. For a basic 1:16 splitting ratio, the distribution network experiences feeder fiber loss and an approximate insertion loss of 24 dB due to the POS. To assess the applicability of our sensing scheme in PON systems, we scan the launch power (LP) from -24 dBm to 4 dBm. Typical PON systems maintain an input optical power of approximately 4 dBm, which refers to the launch power from the OLT into the feeder fiber. Thus, the sensing probe must operate effectively at LP below -20 dBm (corresponding to a 1:16 splitter ratio) to ensure compatibility with practical deployment conditions. We employ phase variance (PV) in the far-end fiber section as the sensing performance metric, with results presented in Fig. 4(c). For both continuous and pulse LFM probes, the PV remains lower than 0.02 at LP beyond -20 dBm, while the QPSK probe is unable to detect the vibration at LP below -12 dBm. When LP is set below -20 dBm, the PV increases

Optics EXPRESS

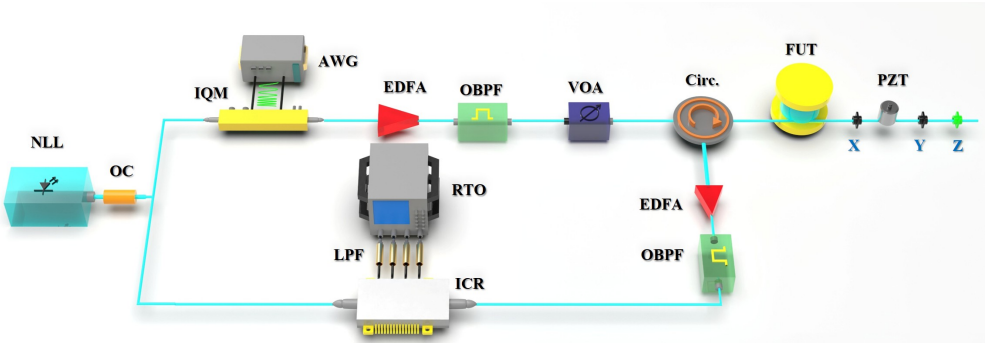

Fig. 2. P2P experimental setup. NLL: narrow linewidth laser, VOA: variable optical attenuator, OC: optical coupler, IQM: IQ modulator, AWG: arbitrary waveform generator, EDFA: erbium-doped fiber amplifier, OBPF: optical bandpass filter, Cir: circulator, PZT: piezoelectric transducer, ICR: integrated coherent receiver, LPF: electrical low-pass filter, RTO: real-time oscilloscope, FUT: fiber under test.

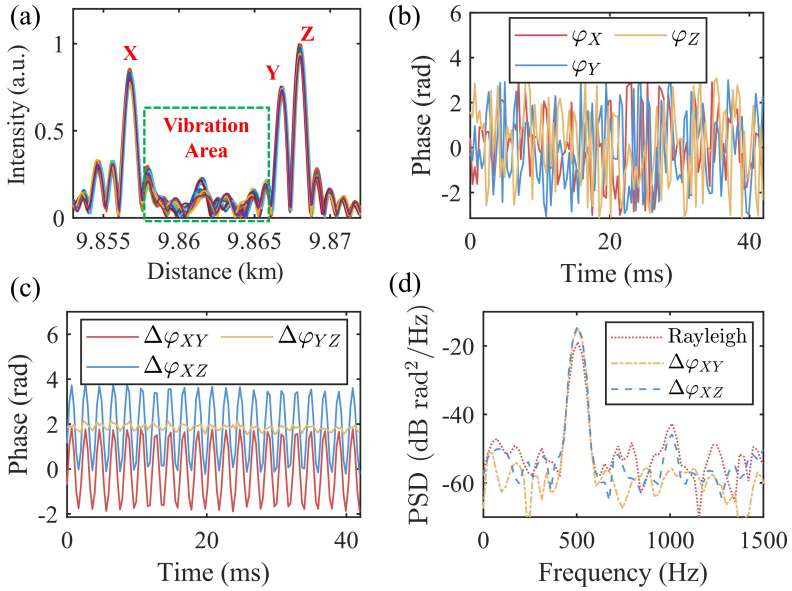

Fig. 3. (a) Intensity traces around vibration area.(b) Phase traces at connector points X, Y and Z.(c) Phase difference among three connector points.(d) PSD curves of the vibration waveforms from $\Delta\varphi_{XY}$, $\Delta\varphi_{XZ}$ and φ-OTDR.

significantly. The obvious fading appears in the trace as shown in Fig. 5(c), which complicates vibration event localization due to distorted phase distribution and low SNR in the RBS trace. However, Fresnel reflection-based detection, which leverages stronger reflection peaks compared to Rayleigh scattering, enables reliable event detection even at low launch powers, with the Fresnel peak at −24 dBm exceeding the noise floor by 6.4 dB, as illustrated in Fig. 5(d). Table 1 compares these three probes in both RBS-based sensing and Fresnel reflection-based sensing. Notably, at LP = −20 dBm, all three probes produce strong Fresnel reflection peaks, allowing vibration detection via phase difference calculations.

Optics EXPRESS

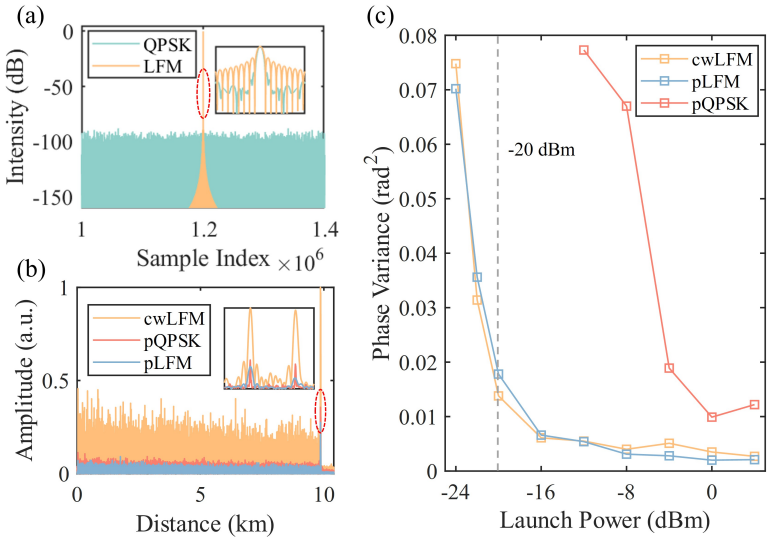

Fig. 4. (a) ACFs of the LFM probe and QPSK probe with the same 500-MHz bandwidth.(b) RBS traces after matched filtering of the continuous LFM probe, LFM pulse probe, and QPSK pulse probe, respectively. (c) PV of the RBS trace at the 10-km fiber end induced by continuous LFM probe, LFM pulse probe, and QPSK pulse probe, respectively.

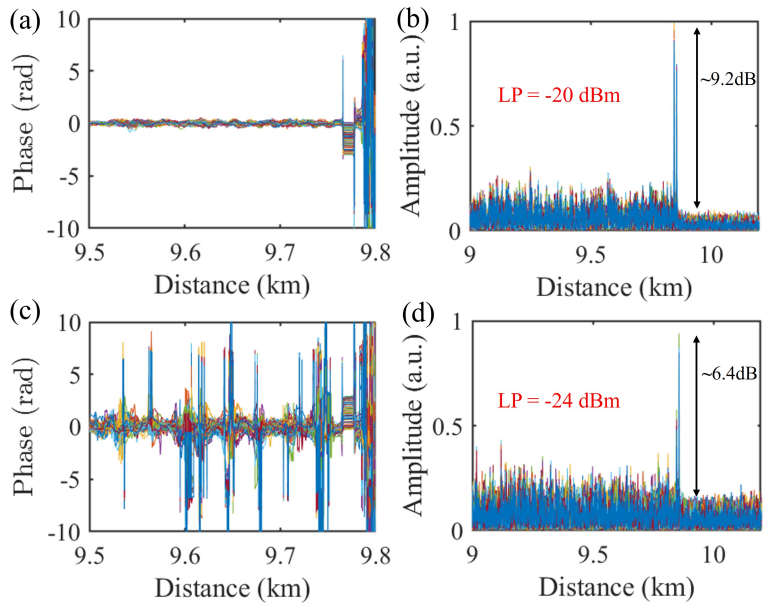

Fig. 5. (a) Phase traces and (b) RBS traces after matched filter when LP is set to −20 dBm. (c) Phase traces and (d) RBS traces after matched filter when LP is set to −24 dBm.

Table 1. Comparison of Probe Types in φ-OTDR System at LP = −20 dBm

Probe Type	Duty Cycle	PV from DFOS (rad^2)	Peak-to-noise ratio (dB)
QPSK Pulse	~3.03%	/	8.9
LFM Pulse	~3.03%	0.0178	9.7
Continuous LFM	100%	0.0138	9.2

Optics EXPRESS

3.2. P2MP experiment

Having validated that continuous and pulse LFM probes achieve a sensing dynamic range suitable for structures, we will next investigate the performance of the continuous LFM probe in multi-branch event detection. We experimentally evaluate the sensing performance of the system in PON, as illustrated in Fig. 6. The system comprises a feeder fiber connected to a POS followed by four branch fibers, emulating a P2MP architecture. A 1-m PZT is placed at the end of the feeder fiber, applying a 500 Hz vibration with a peak-to-peak amplitude of 2 Vpp. The transmitter and receiver configurations remain consistent with those described in Fig. 2. Table 2 presents the optical power at points A, B, C, and D under the experimental conditions. Four different events are emulated across the four branches: (1) in Branch #1, a 255-meter fiber is placed in a chamber for heating to monitor temperature changes; (2) Branch #2 introduces a fiber breakpoint; (3) Branch #3 is subjected to fiber bending; and (4) Branch #4 is deployed with a 10-m PZT to apply a 500 Hz vibration. All fibers in branches are connected by UPC connectors, while APC connectors are located at the end of each branch. Fiber connectors in each branch are systematically labeled according to their distance from the POS. For instance, in Branch #1, the connectors are designated as #1-1 (UPC), #1-2 (UPC), and #1-3 (APC). At point D, the signal received from the circulator comprises the RBS signals from both the feeder fiber and branches, as well as the Fresnel reflection signals from the reflection reflectors within each branch. The actual positions of the components are shown in Fig. 7. Figure 8(a) presents the intensity trace after matched filter, consisting of RBS and Fresnel reflection signal. Offline DSP is adopted to estimate dynamic variations in optical phase at every fiber position along the feeder fiber. The signal is processed by the RVS algorithm, which segments the trace into five sub-traces to suppress interference fading, achieving a theoretical spatial resolution of 1 m. Following this, we employ the moving rotated-vector-average (MRVA) method to conduct a sliding average [25], further reducing fading effects. The phase waterfall plot is shown in Fig. 8(b), with few fading points along the feeder fiber. According to the phase variance illustrated in Fig. 8(c), the spatial resolution is 1 m. The vibration waveform and corresponding PSD curve are depicted in Fig. 8(d), revealing a noise floor around -49 dB rad^2/Hz, corresponding to a sensing sensitivity of 56 p$\varepsilon/\sqrt{\text{Hz}}$. Additionally, we perform continuous sampling of 64 traces of feeder fiber and apply an initial averaging step, yielding a trace that displays the typical features of an OTDR trace along with a peak mainly induced by the Fresnel reflection of the POS, as illustrated in Fig. 9(a). We then carry out measurements over a 1-hour duration to obtain the final averaged trace, as shown in Fig. 9(b). From this curve, the LPP of the feeder fiber is extracted, enabling us to estimate the attenuation coefficient, which is calculated to be 0.207 dB/km.

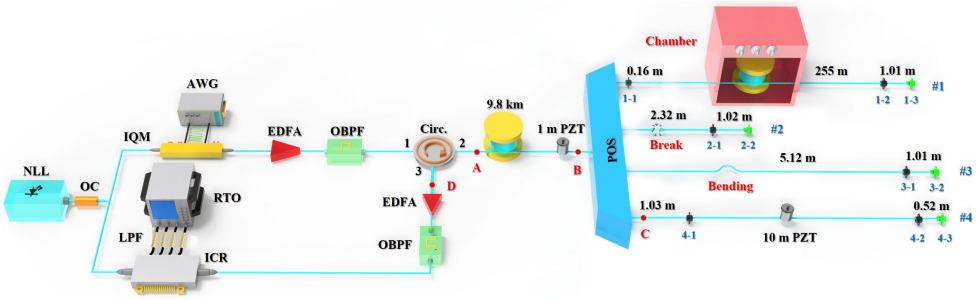

Fig. 6. P2MP experimental setup.

The traces after passing through the POS are excluded to process branch recognition and extract corresponding events. 50 consecutive intensity traces are averaged to enhance measurement precision, as illustrated in Fig. 10(a). The yellow curve represents the trace before perturbations,

Optics EXPRESS

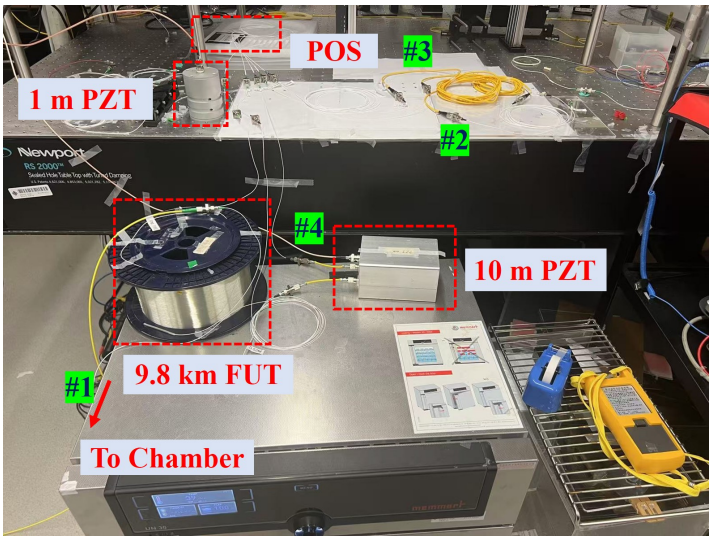

Fig. 7. Photograph of the actual experimental system, where Branch #1 contains a coil of fiber placed in a chamber to simulate power variations due to heating, Branch #2 has a severed fiber to mimic a breakpoint, Branch #3 features a bent fiber, and Branch #4 uses a 10 m PZT to simulate vibration.

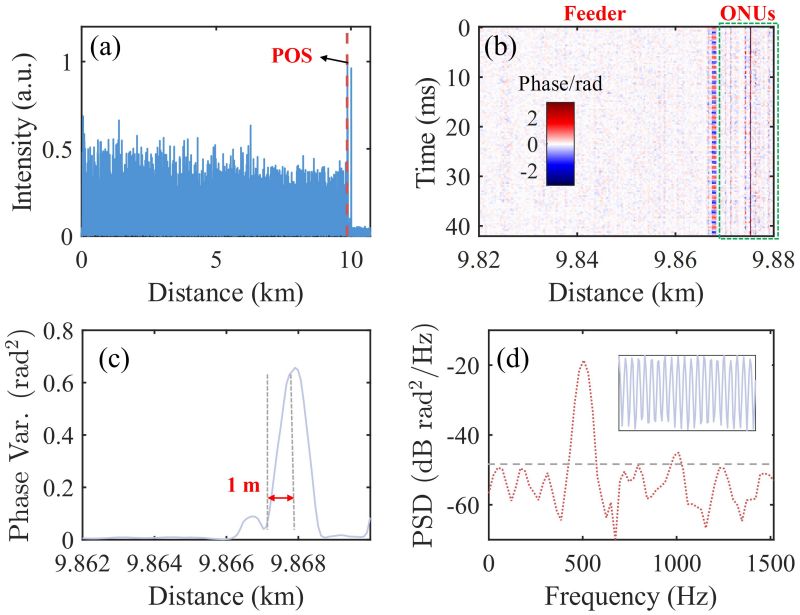

Fig. 8. (a) Backscattering intensity trace.(b) Phase waterfall plot near the vibration area.(c) Phase variance at the identified vibration area.(d) Vibration waveform and its PSD curve.

Table 2. Measured optical powers at 4 points.

Points	A	B	C	D
Power (dBm)	2.11	0.03	−6.45	−32.41

Optics EXPRESS

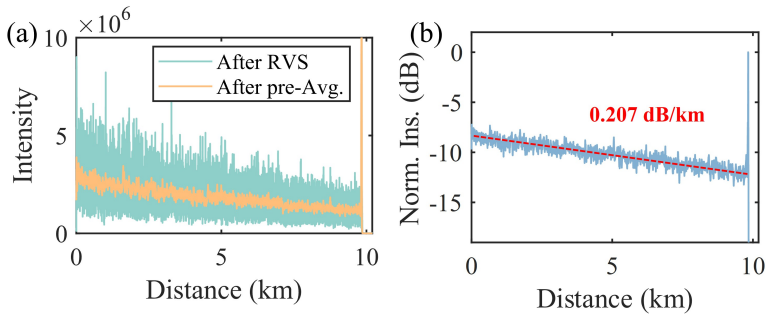

Fig. 9. (a) RBS trace after RVS and the pre-averaged trace after MRVA.(b) Estimated LPP of the feeder fiber after averaging for 1 hour.

while the blue curve corresponds to the trace after perturbations. A magnified view is presented in Fig. 10(b), revealing a spatial resolution of 0.2 m derived from the FWHM of the averaged peak. The correlation peaks correspond to the signals reflected by each fiber connector, with their arrival order and time intervals determined by the differences in their respective lengths. Each ONU branch is uniquely identified by the positions and intensities of its Fresnel reflection peaks, which serve as distinctive markers for branch recognition in the overlapped trace. After applying perturbations, the Fresnel reflection peaks at connectors #2-1 and #2-2 disappear, indicating a fiber break in the branch #2. This disappearance suggests that the optical path in the branch #2 has been interrupted, preventing the reflection of light back to the sensing end. And the Fresnel reflection peaks at connectors #3-1 and #3-2 exhibit an intensity reduction of approximately 3 dB. This attenuation can be attributed to bending-induced loss in the branch #3.

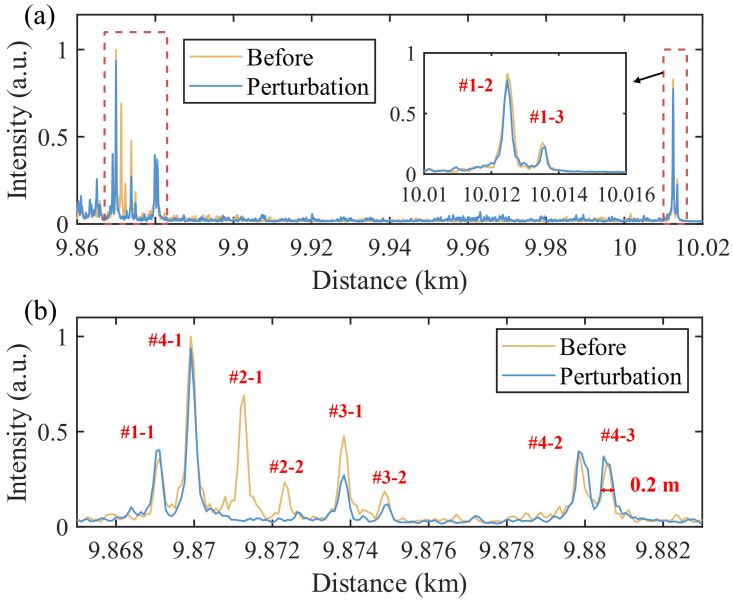

Fig. 10. (a) Intensity traces before and after perturbation in the area of ONU branches. The zoom-in plot indicates the traces near connector points #1-2 and #1-3. (b) Zoom-in plot of the intensity traces from 9.867 km to 9.883 km.

Optics EXPRESS

Furthermore, temperature monitoring is conducted for branch #1 utilizing connectors #1-1 and #1-2. The temperature chamber is programmed to heat a 255-m fiber from 40°C to 55°C over 5 minutes. The phase difference between reference reflectors arises because the temperature-induced change in the refractive index alters the optical path length, thereby affecting the relative phase of the reflected signals detected at the sensing end. The phase traces of two reference connectors and the difference trace are measured within a 256-ms time window, as depicted in Figs. 11(a) and 11(b). The phase difference demonstrates an approximately linear temporal relationship, with a linear fit yielding a slope $d\varphi/dt$ of 755.34 rad/s. The corresponding phase-temperature coefficient is determined to be 15.11 rad/mK, and the refractive index-temperature coefficient dn/dt is calculated as 7.31×10^{-6} K^{-1} based on Eq. (4). For branch #4, vibration detection is achieved based on the phase difference between connectors #4-1 and #4-2. The phase traces are illustrated in Fig. 11(c) and the difference trace indicates the waveform. We also detect the vibration when disconnecting other branches, showing negligible deviation in both the P2MP and P2P scenarios. Additionally, vibrations at various frequencies are measured, and the corresponding PSD curves are shown in Fig. 11(d), with a noise floor of −44 dB rad^2/Hz and a sensing sensitivity of 93 $p\varepsilon/\sqrt{Hz}$.

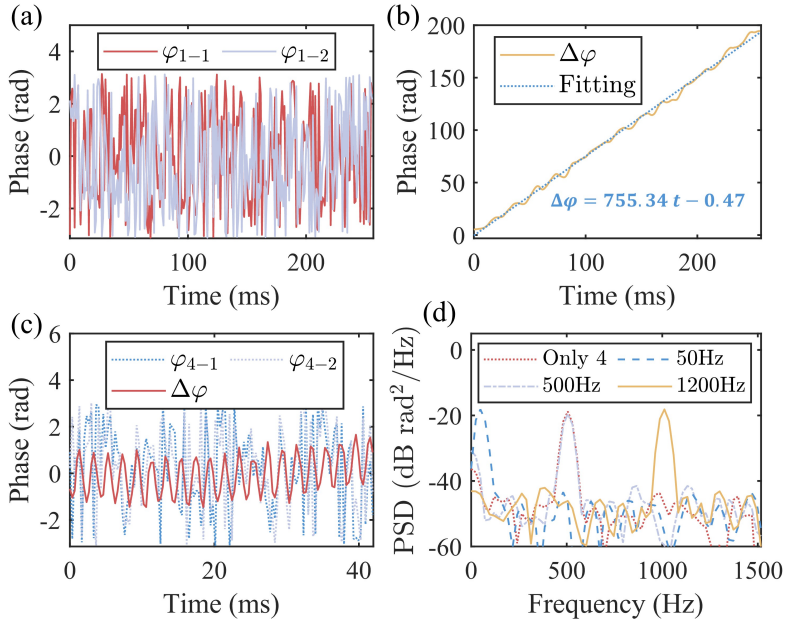

Fig. 11. (a) Phase trace between connector points #1-1 and #1-2.(b) Phase difference between connector points #1-1 and #1-2 and the fitted line.(c) Phase trace between connector points #4-1 and #4-2, and their phase difference.(d) PSD of the phase differences when applying vibration of different frequencies and disconnecting other branches.

3.3. *In-service monitoring*

To enable effective in-service PON monitoring, our proposed continuous LFM-based φ-OTDR scheme can be implemented in two distinct ways. On the one hand, the continuous LFM probe can serve as the communication carrier for simultaneous sensing and data transmission [26]. However, it necessitates precise optical filtering to generate a pure LFM carrier, ensuring minimal influence on communication signals. On the other hand, a separate communication channel can be dedicated exclusively for a continuous LFM probe to achieve in-service monitoring. In this configuration, the continuous LFM probe demonstrates significant advantages over its pulse

Optics EXPRESS

LFM counterpart. Specifically, the continuous LFM probe maintains a low peak power, which prevents abrupt power variations that could induce fiber nonlinearities, thereby preserving the integrity of the communication channel. In contrast, pulse LFM probes, due to their inherent power transients, may excite nonlinear effects that interfere with data transmission. To mitigate this, pulse LFM probes require careful pulse shaping of the rising and falling edges to reduce the impact of power surges [27]. Furthermore, in typical PON deployments with short-distance feeder fiber, phase noise accumulation has a negligible effect on the sensing probe, reinforcing the suitability of continuous LFM probes for robust in-service monitoring.

To evaluate the effectiveness of our proposed scheme, we compared it against existing PON monitoring approaches, with the results summarized in Table 3. Our proposed scheme, utilizing a continuous LFM probe, achieves superior performance in PON monitoring compared to alternative approaches, such as those based on PRBS [7], ultra-long PN sequence [20], and conventional OTDR [28]. Specifically, it enables DFOS along the feeder fiber, leveraging the high phase sensitivity of the continuous LFM probe to detect events with enough power margin (> 24 dB), as demonstrated in Fig. 4(c). Simultaneously, the scheme supports branch recognition in multi-branch PON architectures and the event detection of fiber breaks, bending, strain, and temperature changes at ONU branches. Additionally, the continuous LFM probe potentially can reduce the impact on the communication channel by avoiding a high peak-to-average power ratio, which could cause fiber nonlinearities. However, our proposed method with the NLL increases the cost compared to electroabsorption modulated laser (EML) or conventional OTDR-based solutions [20,28]. To address this, future implementations could employ an integrated tunable laser assembly (ITLA) combined with phase noise compensation techniques to reduce costs [29].

Table 3. Comparison of Sensing Schemes for PON Monitoring

Criterion	Proposed Method	Ref. [7]	Ref. [20]	Ref. [28]
Sensing Probe	CW LFM	PRBS Sequence	PN Sequence	Single Pulse
Laser Type	NLL	NLL	EML	Fabry-Pérot
DFOS of feeder fiber	Yes	No	No	No
Branch Recognition	Yes	No	Yes	Yes
Break/Bend	Yes	Yes	Yes	Yes
Strain/Temperature	Yes	Yes	No	No

4. Conclusion

In conclusion, we propose a novel continuous LFM-based φ-OTDR scheme that significantly advances in-service PON monitoring. Our primary contribution lies in the integration of distributed sensing along the feeder fiber and Fresnel reflection-based monitoring of multiple ONU branches. We find that Fresnel reflection-based sensing performs consistently across continuous LFM, pulsed LFM, and pulsed QPSK probes, whereas φ-OTDR excels with the continuous LFM probe due to its high sensing sensitivity and compatibility with existing PON structure. In a P2MP scenario, the feeder fiber achieves a spatial resolution of 1 m with fading-free distributed sensing, enabling reliable detection of LPP by long-period averaging. Meanwhile, the ONU branches are recognized and monitored via Fresnel reflections of reference reflectors, achieving a higher spatial resolution of 0.2 m. Our scheme supports effective detection of breakpoints, bending, vibrations, and temperature changes in ONU branches. Additionally, the proposed scheme is fully compatible with existing PON infrastructure by employing the continuous LFM probe as the communication carrier or by allocating a dedicated wavelength for sensing. In the future, we plan to develop phase noise compensation techniques to reduce costs primarily associated with NLL.

Optics EXPRESS

Funding. National Key Research and Development Program of China (2023YFB2905300).

Disclosures. The authors declare no conflicts of interest.

Data Availability. Data underlying the results presented in this paper are not publicly available at this time but may be obtained from the authors upon reasonable request.

References

1. T. Koonen, "Fiber to the home/fiber to the premises: What, where, and when?" in *Proceedings of the IEEE*, (2006).
2. M. M. Rad, K. Fouli, H. A. Fathallah, *et al.*, "Passive optical network monitoring: Challenges and requirements," IEEE Commun. Mag. **49**(2), s45–S52 (2011).
3. F. Caviglia and V. C. D. Biase, "Optical maintenance in pons," in *ECOC*, (1998), pp. 621–625.
4. M. A. Esmail and H. Fathallah, "Physical layer monitoring techniques for tdm-passive optical networks: A survey," IEEE Commun. Surv. Tutorials **15**(2), 943–958 (2013).
5. F. Azendorf, A. Sandmann, and M. Eiselt, "Pressure wave detection and localization in deployed underground fiber using coherent correlation otdr," in *OFC*, (2024), p. M2K.3.
6. M. Eiselt, A. Sandmann, and F. Azendorf, "Simultaneous temperature and acoustic sensing with coherent correlation otdr," in *OFC*, (2023), p. W3J.3.
7. F. Azendorf, A. Sandmann, W. Reimer, *et al.*, "Acoustic sensing after 50 km of transmission fibre using coherent optical subassembly," in *ECOC*, (2023), pp. 920–923.
8. E. Ip, J. Fang, Y. Li, *et al.*, "Distributed fiber sensor network using telecom cables as sensing media: technology advancements and applications [invited]," J. Opt. Commun. Netw. **14**(1), A61–A68 (2022).
9. C. Dorize, S. Guerrier, E. Awwad, *et al.*, "Capturing acoustic speech signals with coherent mimo phase-otdr," in *ECOC*, (2020), pp. 1–4.
10. G. A. Wellbrock, T. J. Xia, M.-F. Huang, *et al.*, "Explore benefits of distributed fiber optic sensing for optical network service providers," J. Lightwave Technol. **41**(12), 3758–3766 (2023).
11. S. Wang, X. Fan, Q. Liu, *et al.*, "Distributed fiber-optic vibration sensing based on phase extraction from time-gated digital ofdr," Opt. Express **23**(26), 33301–33309 (2015).
12. P. Li, Y. Wang, P. Wang, *et al.*, "Pulse coding in distributed optical fiber vibration sensor: A review," IEEE Sens. J. **21**(20), 22371–22387 (2021).
13. H. Martins, K. Shi, B. Thomsen, *et al.*, "Real time dynamic strain monitoring of optical links using the backreflection of live psk data," Opt. Express **24**(19), 22303–22318 (2016).
14. M. Liu, J. Wang, L. Chen, *et al.*, "Integration of communication and distributed sensing over optical supervisory channel using live qpsk streams," Opt. Lett. **50**(4), 1409–1412 (2025).
15. M. Thollabandi, T. Y. Kim, S. Hann, *et al.*, "Tunable otdr based on direct modulation of self-injection-locked rsoa for in-service monitoring of wdm-pon," IEEE Photonics Technol. Lett. **20**(15), 1323–1325 (2008).
16. W. Chen, B. Mulder, J. Vandewege, *et al.*, "Embedded otdr monitoring of the fiber plant behind the pon power splitter," in *Proceedings of the IEEE*, (2006).
17. K. Abdelli, K. Abdelli, C. Tropschug, *et al.*, "Branch identification in passive optical networks using machine learning," in *OFC*, (2023), p. M2G.4.
18. Z. Zhong, W. Liu, H. Li, *et al.*, "Pon monitoring based on dual-fbg periodic encoders and sequence correlation," in *ACP/POEM*, (2023).
19. H. Fathallah, M. M. Rad, and L. A. Rusch, "Pon monitoring: Periodic encoders with low capital and operational cost," IEEE Photonics Technol. Lett. **20**(24), 2039–2041 (2008).
20. Z. Zhong, W. Liu, M. Luo, *et al.*, "Correlation-based otdr for high-resolution monitoring in passive optical networks," in *OFC*, (2024), p. M1K.2.
21. Y.-K. Huang and E. Ip, "Simultaneous optical fiber sensing and mobile front-haul access over a passive optical network," in *2020 Optical Fiber Communications Conference and Exhibition (OFC)*, (2020), pp. 1–3.
22. D. Chen, Q. Liu, and Z. He, "Phase-detection distributed fiber-optic vibration sensor without fading-noise based on time-gated digital ofdr," Opt. Express **25**(7), 8315–8325 (2017).
23. Y. Dong, X. Chen, E. Liu, *et al.*, "Quantitative measurement of dynamic nanostrain based on a phase-sensitive optical time domain reflectometer," Appl. Opt. **55**(28), 7810–7815 (2016).
24. J. S. Wey, "The outlook for pon standardization: A tutorial," J. Lightwave Technol. **38**(1), 31–42 (2020).
25. H. Qian, B. Luo, H. He, *et al.*, "Fading-free ϕ-otdr evaluation based on the statistical analysis of phase hopping," Appl. Opt. **61**(23), 6729–6735 (2022).
26. H. He, L. Jiang, Y. Pan, *et al.*, "Integrated sensing and communication in an optical fibre," Light: Sci. Appl. **12**(1), 25 (2023).
27. M. A. Allousch and A. Sandmann, "Cc-otdr sequence shaping enabling joint co-directional sensing and communication," arXiv (2025).
28. P. J. Urban, "Mitigation of the parallel-path effect for reliable monitoring of a passive optical network using standard optical time domain reflectometry," J. Opt. Commun. Netw. **15**(10), 776–782 (2023).
29. Z. Xiao, J. Chen, J. Ji, *et al.*, "Complete phase noise compensation for 50 km das with 100 khz linewidth itla," in *28th International Conference on Optical Fiber Sensors*, (2023), p. F2.1.